Appl. Phys. B 83, 43–50 (2006)
DOI: 10.1007/s00340-005-2068-y

**Applied Physics B**
**Lasers and Optics**

M. GERBER[1,✉]
T. GRAF[2]
A. KUDRYASHOV[3]

# Generation of custom modes in a Nd:YAG laser with a semipassive bimorph adaptive mirror

[1] Institute of Applied Physics, University of Bern, Sidlerstrasse 5, 3012 Berne, Switzerland
[2] Institut für Strahlwerkzeuge, University of Stuttgart, Pfaffenwaldring 43, 70569 Stuttgart, Germany
[3] Adaptive Optics for Industrial and Medical Applications Group, Adopt Ltd, Dm. Ulyanov str. 4-2-13, Moscow 119333, Russia

**Received: 21 March 2005 / Revised version: 10 October 2005**
**Published online: 4 February 2006 •** 

**ABSTRACT** Custom modes at a wavelength of 1064 nm were generated with a deformable mirror. The required surface deformations of the adaptive mirror were calculated with the Collins integral written in a matrix formalism. The appropriate size and shape of the actuators as well as the needed stroke were determined to ensure that the surface of the controllable mirror matches the phase front of the custom modes. A semipassive bimorph adaptive mirror with five concentric ring-shaped actuators and one defocus actuator was manufactured and characterised. The surface deformation was modelled with the response functions of the adaptive mirror in terms of an expansion with Zernike polynomials. In the experiments the Nd:YAG laser crystal was quasi-CW pumped to avoid thermally induced distortions of the phase front. The adaptive mirror allows to switch between a super-Gaussian mode, a doughnut mode, a Hermite-Gaussian fundamental beam, multi-mode operation or no oscillation in real time during laser operation.

**PACS** 42.60.Jf; 42.60.Da; 42.60.By

## 1 Introduction

For every application there is an ideal intensity distribution which yields optimum results. Such intensity distributions of the beam are commonly called custom modes because their spatial shape is optimised for a specific purpose. Either the special shape of the beam is advantageous for the generation of the laser radiation inside the cavity or for the laser induced process on a target. Due to their high potential in numerous applications we discuss the super-Gaussian mode (also known as top-hat or flat-top mode) and the doughnut mode as two examples of custom modes in the following.

The super-Gaussian mode is characterised by a homogeneous intensity distribution and steep edges whereas the doughnut mode exhibits a ring shape with vanishing intensity in the centre of the beam. The intensity distributions of the super-Gaussian mode $I_{\mathrm{SG}}(r)$ and the doughnut mode [1] $I_{\mathrm{DN}}(r)$ are given by

$$I_{\mathrm{SG}}(r) = I_0 \mathrm{e}^{-2\left(\frac{|r|}{w_0}\right)^n} \quad \text{with} \quad n > 2 \tag{1}$$

$$I_{\mathrm{DN}}(r) = 2I_0 \left(\frac{r}{w_0}\right)^2 \mathrm{e}^{-2\left(\frac{r}{w_0}\right)^2}, \tag{2}$$

✉ Fax: ++41(0)31 340 8280, E-mail: migerber@bluewin.ch

where $I_0$ is the peak intensity, $w_0$ is the radius of the mode and $n$ is the super-Gaussian index or – in other words – the order of the super-Gaussian beam. The intensity distributions of the modes are shown in Fig. 1 as solid line for the super-Gaussian mode and as dashed line for the doughnut beam.

The beam propagation factor $M^2$ of the fundamental super-Gaussian mode is given by [2–4]

$$M^2 = \left[\frac{n}{4}2^{4/n}\frac{\Gamma\left(\frac{1}{2}+\frac{2}{n}\right)}{\Gamma\left(\frac{1}{2}\right)\Gamma\left(1+\frac{2}{n}\right)}\right]^{1/2} \tag{3}$$

with $\Gamma(x)$ being the Gamma function. A super-Gaussian beam with a super-Gaussian index of $n = 6$ features a $M^2$ factor of 1.3, which is slightly higher than the $M^2$ value of the fundamental Hermite–Gaussian beam ($n = 2$, $M^2 = 1$). But even for a super-Gaussian mode with a super-Gaussian index of 15 the beam propagation factor $M^2$ is less than 2.

Many applications benefit from custom-shaped mode profiles: In material processing, for instance, the steep slopes of the intensity profile of the super-Gaussian beam result in sharper edges of the treated workpiece and less rework is ne-

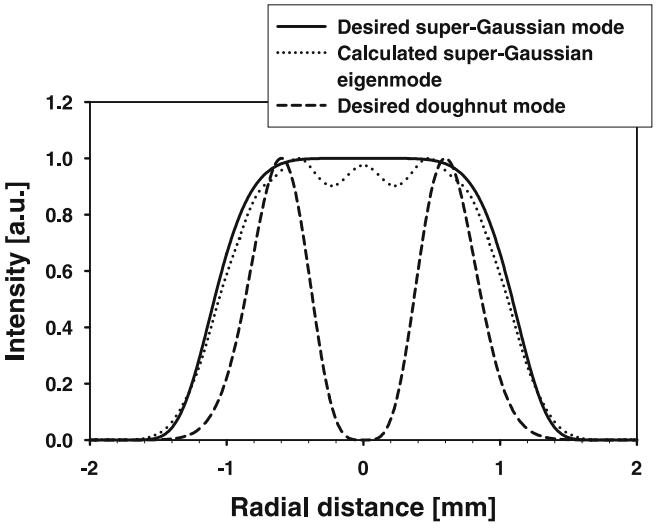


**FIGURE 1** Desired ideal super-Gaussian mode of the sixth order (*solid line*) and the calculated eigenmode for the cavity with the (non-ideal) adaptive mirror (*dotted line*). The normalized doughnut intensity distribution is shown as a *dashed line*

cessary. When a pressure gradient is needed to remove the fused material the $TEM_{00}$ Gaussian mode is the appropriate beam however. Custom modes can also be used for the hardening of metal surfaces [5]. For the generation of higher harmonics in the field of non-linear optics a flat-topped intensity profile ensures optimum frequency conversion efficiencies below the damage threshold of the non-linear crystal [6]. The optimum pump distribution to minimise thermally induced lenses, birefringence, and stress is the homogeneous pump distribution. Hence, to reach high extractions efficiency in a homogeneously pumped laser medium, a super-Gaussian laser beam offers the best overlap with the gain medium. The super-Gaussian beam does not in principle feature a larger mode volume, but a Gaussian mode with the same large radius would suffer from losses due to the truncated wings of the beam. Consequently a super-Gaussian mode with the appropriate beam width is to be favoured also for this reason [7]. Optical tweezers have gained significant importance for the manipulation of organic material. Among Bessel beams the doughnut mode is especially useful to trap large and nontransparent particles.

To generate custom modes one has to modify the phase of the propagating wave inside the resonator. When the profile on a beam shaping element matches the phase front of the custom mode the amplitude is reconstructed after one round trip as sketched in Fig. 2. Typically the wave front of a propagating custom mode features a spherical curvature with small deviations. These modulations of the phase front are in the order of about one tenth of the laser wavelength.

The phase inside the cavity can be modulated with phase plates, or so-called graded-phase mirrors [8–10]. Diffractive optical elements were also successfully applied, but the required structures are more complex as compared to graded-phase mirrors [11]. For $CO_2$ lasers, graded-phase mirrors can easily be manufactured with diamond turning machining due to its comparatively large wavelength of $\lambda = 10.6\,\mu m$ [12, 13]. With the vapour deposition technique and an appropriate mask, we manufactured a graded-phase mirror for the ten times shorter wavelength of a Nd:YAG laser and generated super-Gaussian modes of the sixth order [14].

However a graded-phase mirror or other static beam shaping optics are designed for a specified cavity and a single, defined custom mode. For the real-time control of the spatial shape of the oscillating modes adaptive means are desirable.

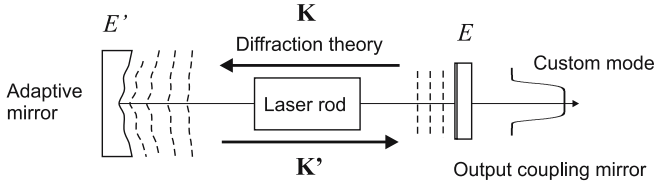


**FIGURE 2** The custom mode $\boldsymbol{E}$, e.g., a super-gaussian mode, is specified at the position of the output coupling mirror. Its plane phase front is drawn as a *dashed line*. The phase front of the field $\boldsymbol{E}'$ (drawn as *dashed line*) at the position of the adaptive mirror can be found by propagating the electromagnetic field $\boldsymbol{E}$ through the cavity by using diffraction theory (Collins integral written in terms of a matrix $\boldsymbol{K}$). When the profile of the beam shaping mirror coincides with the phase front of the incident beam, the desired custom mode is reconstructed after one round trip

When varying beam shapes are needed, an adaptive mirror can spare the exchange and the readjustment of the different beam shaping optics. An adaptive mirror can change the phase front inside the cavity in real-time. In addition, with an adaptive mirror it is also possible to simultaneously correct for the varying thermal distortions of the beam passing through an aberrated gain medium. An adaptive mirror is, therefore, a very versatile beam shaping device.

Nowadays adaptive mirrors are widespread in terrestrial astronomic telescopes to correct the aberrations caused by atmospheric turbulences and become more and more popular in laser optics. Adaptive mirrors were already successfully used to reduce the aberrations of a beam transmitted through large glass amplifiers of high energy laser facilities [15] or to improve the beam quality in high-power solid state oscillators [16–18] or MOPAs [19] operating in the multimode regime. Further applications of deformable mirrors include efficient coupling of light into an optical single-mode fiber [20] and retinal imaging of the human eye [21]. The successful generation of super-Gaussian beams in $CO_2$ lasers with adaptive mirrors was reported in [22]. The approximately ten times shorter wavelength of the Nd:YAG laser, however, requires a higher quality of the mirror polishing and a higher resolution of the actuator stroke. In this paper we present the formation of super-Gaussian and doughnut beams at a wavelength of 1064 nm by means of a semi-passive bimorph adaptive mirror.

In Sect. 2 we first discuss the calculation of the necessary surface deformation of the deformable mirror to generate custom modes. In Sect. 3 the layout of the custom designed controllable mirror is described in detail and in Sect. 4 it is shown how the deformable surface of the mirror can be modelled by means of a linear expansion of response functions. The experimental results are presented in Sect. 5.

## 2 Calculation of the needed surface deformation of the adaptive mirror

To find the profile on the adaptive mirror that is required to generate a custom mode, we start with the desired amplitude distribution of the custom mode at the flat output coupling mirror (plane phase front), and calculate the propagation of the mode through the cavity to get the phase distribution of the electric field at the position of the beam shaping mirror (see Fig. 2) [23, 24]. When the surface profile of the adaptive mirror matches the phase front of the beam the mirror conjugates the phase of the incident electric field. After the propagation back through the cavity the field shows again a plane phase front at the position of the flat output coupling mirror and the initial amplitude distribution of the custom mode is recovered after one round-trip. Thus the field represents an eigenmode of the resonator.

For the calculation of the field propagation through the cavity it is convenient to use the Collins integral. It is a generalised Kirchhoff integral and it allows to consider optical elements in the propagation path represented by ray transfer matrices. As shown in [14] the Collins integral can be approximated with a complex propagation matrix $\boldsymbol{K}$. The electric field $\boldsymbol{E}'$ at the position of the adaptive mirror can then be written as a multiplication of a matrix $\boldsymbol{K}$ (Collins kernel) and a vector $\boldsymbol{E}$,

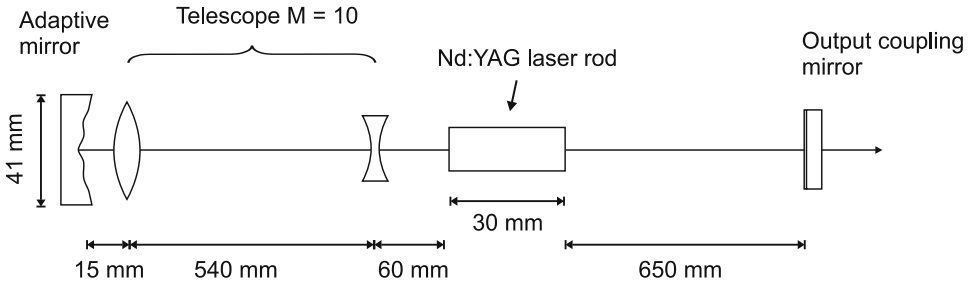


**FIGURE 3** Setup for the measurements with the adaptive mirror. An intracavity Galilei telescope enlarged the beam at the position of the adaptive mirror

which represents the radial field distribution at the location of the flat output coupler:

$$\boldsymbol{E}' = \boldsymbol{K}\boldsymbol{E}\,. \tag{4}$$

The argument of the complex field $\arg(\boldsymbol{E}')$ yields the phase front of the custom mode at the position of the beam shaping mirror and therewith the profile of the adaptive mirror. When the profile of the adaptive mirror matches the phase front $\arg(\boldsymbol{E}')$ the custom mode amplitude $|\boldsymbol{E}|$ is reconstructed.

With this method the profile of a deformable mirror which generates a super-Gaussian mode of the sixth order ($n = 6$, $w_0 = 1.3$ mm) was calculated. We have chosen the super-Gaussian mode as an example of a custom mode due to its high potential in numerous applications. The cavity which was used in the experiments defined the ray transfer matrix. As shown in Fig. 3 the resonator consisted of the adaptive mirror on one end, followed by a telescope and the laser rod and a plane output coupler on the other end.

The distances between the individual optical elements are given in the figure. The optimum mirror surface profile to generate the desired super-Gaussian mode in this cavity is shown as a solid line in Fig. 4.

Despite the optimised flexibility of the adaptive mirror, the ideal shape could not be reproduced exactly. We modelled the mirror surface in terms of the measured response functions (see Sect. 4) to determine how the mirror surface can be adapted to the calculated phase front. As a result the ideal shape was very well approximated by the modelled and the real mirror shape as shown by the dashed and dotted curves in Fig. 4. To examine the influence of the approximation on the intensity distribution of the output beam the eigenmode of the resonator with this approximated mirror surface was calculated. Again we can take advantage of the Collins integral written in the form of a matrix. Now the cavity with its adaptive mirror is given and the eigenmode of the resonator is calculated. The eigenmodes of the cavity are the solutions of the eigenvalue equation

$$\boldsymbol{K}_{\circlearrowleft}\boldsymbol{E} = \gamma\boldsymbol{E} \tag{5}$$

and can easily be calculated with common mathematical software. $\boldsymbol{K}_{\circlearrowleft}$ is the round-trip propagation given by

$$\boldsymbol{K}_{\circlearrowleft} = \boldsymbol{K}'\,\mathrm{e}^{i2\triangle\phi}\boldsymbol{K} \tag{6}$$

with $\boldsymbol{K}$ being a complex matrix, which describes the forward propagation from the output coupling mirror to the adaptive mirror, with $\triangle\phi(r)$ being the profile of the adaptive mirror and $\boldsymbol{K}'$ being the backwards propagation. The factor two in the exponent takes into account that the adaptive mirror causes a local phase shift of twice the depth of the profile.

The intensity distribution of the calculated eigenmode of the resonator with the approximated profile on the adaptive mirror is shown by the dotted line in Fig. 1 and differs only slightly from the desired super-Gaussian mode (see Fig. 1, solid line). The round-trip loss $(1-\gamma^2)$ of the eigenmode in the cavity with the approximated profile on the adaptive mirror was evaluated to be 0.53% for the super-Gaussian mode. The calculated second moment radius of the beam on the adaptive mirror is 12.74 mm. Unexpectedly the optimum profile would cause higher round-trip losses of 0.70%. This behaviour can be explained by the larger calculated beam radius of 12.90 mm on the adaptive mirror resulting in higher diffraction losses at the edge of the mirror.

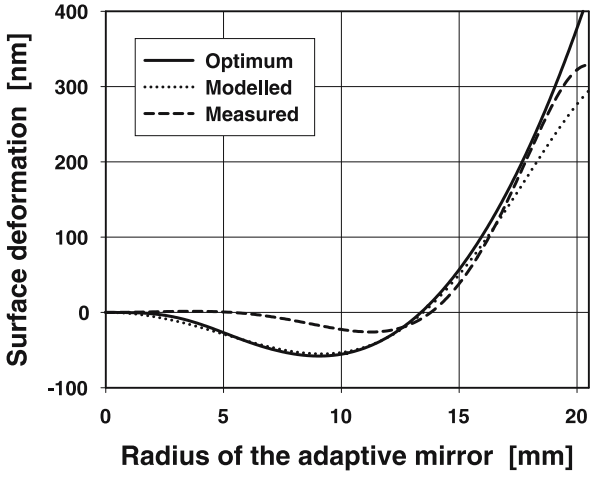


**FIGURE 4** Calculated optimum surface deformation for the generation of the super-Gaussian mode (*solid line*). With an appropriate set of voltages the modelled surface deformation (*dotted line*) almost coincides with the optimum mirror profile. The surface deformation which generated the super-Gaussian beam in the performed experiments was measured with an interferometer (*dashed line*)

## 3 Design of the semipassive bimorph adaptive mirror

A semipassive bimorph adaptive mirror, which is applicable in lasers, typically consists of a piezoceramic disc between two electrodes which is glued on a glass substrate. A HR-coating for the laser wavelength was vapour deposited on the glass substrate. One of the electrodes is divided into several zones, and the other serves as a common ground. With a multi-channel high-voltage power supply a control

voltage can be applied to each zone. By applying a voltage to the electrodes, only the piezoceramic expands perpendicular to the applied electric field and not the glass substrate resulting in a bending of the mirror surface. The stroke of the individual actuators is determined by the applied voltage, the transverse piezo modulus as well as by the stiffness and thickness of the piezoceramic and the glass substrate.

To form custom modes with a deformable mirror one has to determine the appropriate arrangement of the actuators. The suitable shape and size of the electrodes was found by solving the following differential equation which describes the static surface deformation $z(x, y)$ of the semi-passive bimorph adaptive mirror for a given applied electric field $\boldsymbol{E}(x, y)$ [25]:

$$\nabla^2\nabla^2 z(x, y) = \frac{-D\, d_{31}\nabla^2 \boldsymbol{E}(x, y)}{2(1-\nu)}\,, \tag{7}$$

with $\nabla^2$ being the Laplace differential operator

$$\nabla^2 = \frac{\mathrm{d}^2}{\mathrm{dx}^2} + \frac{\mathrm{d}^2}{\mathrm{dy}^2}\,. \tag{8}$$

The parameter $D$ subsumes various geometrical and material properties of the mirror, $d_{31}$ is the transverse piezo modulus and $\nu$ represents the Poisson ratio for the piezo ceramic and the glass substrate. It was considered that the Poisson ratio is equal for both materials. The differential equation (7) was transformed into polar coordinates and the solutions were found. The discussion of the solutions is beyond the scope of this paper and will be published elsewhere. According to the results of these calculations, we decided to use ring-shaped actuators due to the rotational symmetric beams and we defined the width of the individual actuators. We did not consider the thermal distortions inside a CW pumped laser crystal therefore we carried out the experiments with a quasi-CW pumped laser crystal to avoid these thermally induced aberrations. Hence the correction of higher-order angle-dependent aberrations with azimuthal segmented actuators was not needed.

The layout of the deformable mirror which was used in the performed experiments is shown in Fig. 5. This custom designed device was developed and manufactured by the Laboratory of Adaptive Optics for Industrial and Medical Applications in Moscow, Russia. A circular actuator with a diameter of 9 mm is situated in the centre of the adaptive mirror and four electrodes are arranged as concentric rings with the same width of 4 mm in the outer section. The clear aperture of the mirror is 41 mm. An additional piezoceramic disc is glued to the first disc with a third vapour deposited electrode layer which is not subdivided. With this electrode the defocus is directly controllable. As can be seen from Fig. 4 the needed stroke of the actuators is in the range of about 100 nm. To achieve a low sensitivity and therewith such a small stroke the glass substrate was comparatively thick. The thickness of the two piezoceramic discs and the LK-105 glass substrate was 0.4 mm and 5.2 mm, respectively. A low temperature HR-coating was vapour deposited on the glass substrate. The reflectivity is specified to 99.9%.

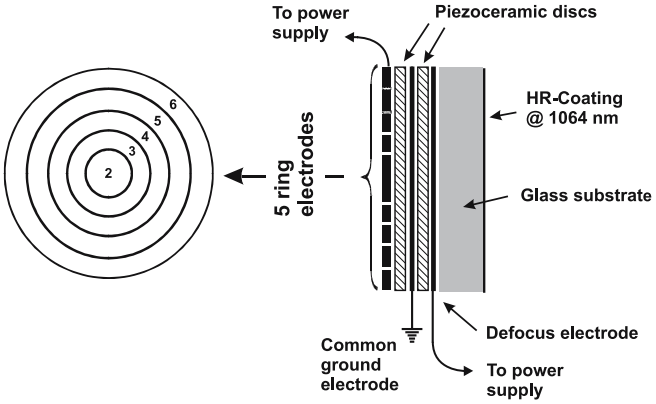


**FIGURE 5** Cross section of the adaptive mirror consisting of two piezoceramic discs sandwiched between three layers of electrodes. The left electrode is subdivided into five concentric rings (Electrodes no. 2 to 6, see scheme on the *left side* of the figure). The electrode (no. 1) on the *right side* is not split up and determines the radius of curvature of the mirror. The electrode in the middle serves as a common ground for the control electrodes

A six-channel high-voltage power supply delivers up to ±150 V with a resolution of 1 V to control the electrodes. The voltages were set manually via a graphical user interface running on a PC. The manufacturer specified the maximum control frequency to 25 Hz.

## 4 Modelling of the mirror surface

To find the appropriate voltage distribution which forms the surface calculated in Sect. 2 the performance of the manufactured mirror has to be modelled. This can be done by measuring the response functions of the actuators. The response functions describe the deformation of the surface caused by a single actuator. These response functions are acquired for every electrode by applying a predefined voltage. The requested surface profile of the adaptive mirror can then easily be modelled as a superposition of scaled response functions.

The response functions of a deformable mirror can be described as an expansion of Zernike polynomials [26–28]. The Zernike polynomials are related to the classical aberrations (e.g., defocus, astigmatism and coma) and, therefore, often utilized to describe wave fronts of laser beams or surfaces of optical elements. For this reason they are also the adequate set of functions to implement complex surface profiles of beam shaping optics with a low number of significant coefficients. By choosing the solutions of the differential equation (7) as a basis the number of significant coefficients would be low as well. But these functions are unusual and without a relation to optics.

Zernike polynomials are a set of complete orthogonal polynomials defined on a unit circle. In polar coordinates they can be written as a product of radial polynomials and angular functions. Here the Zernike polynomials are defined as follows (In this paper we omit the normalization):

$$Z_{\text{even } j} = R_n^m(r)\cos(m\theta) \quad m \neq 0 \tag{9}$$

$$Z_{\text{odd } j} = R_n^m(r)\sin(m\theta) \quad m \neq 0 \tag{10}$$

$$Z_j = R_n^m(r) \quad m = 0 \tag{11}$$

with

$$R_n^m(r) = \sum_{s=0}^{(n-m)/2} \frac{(-1)^s (n-s)!}{s!\,[(n+m)/2-s]!\,[(n-m)/2-s]!} r^{n-2s}. \tag{12}$$

The indices $n$ and $m$ are the radial degree and the azimuthal frequency, respectively. $j$ is a mode-ordering number. The index $m$ has to be smaller or equal $n$ and $n-m$ should be even. Due to the arrangement of the electrodes with concentric rings the deformation of the surface is rotational symmetric. Therefore, only the Zernike polynomials which do not depend on the angle $\theta$ are required. Hence the azimuthal frequency $m$ is always zero. Only (11) will be used and with the simplified equation (12) the angle-independent Zernike polynomials with the radial degree $n$ reads:

$$Z_n(r) = \sum_{s=0}^{n/2} \frac{(-1)^s (n-s)!}{s!\,[(n/2-s)!]} r^{n-2s}. \tag{13}$$

The first five angle-independent Zernike polynomials are listed in Table 1 with their corresponding names known from the classical aberration theory.

The response functions $F_i(r)$ i.e., the surface deformation which is caused by exciting a single actuator can now be written as an expansion of Zernike polynomials:

$$F_i(r) = \sum_{k=1}^{\infty} c_{ik} Z_{2k}(r) - z_0(r), \tag{14}$$

where $i$ is an index for the electrodes, $c_{ik}$ are the Zernike coefficients and $z_0(r)$ is the initial surface i.e., the surface deformation without any voltage applied. We considered the three lowest order coefficients to describe the deformed surface. The response functions were acquired for both the backward and forward deflection of the mirror surface. The response functions of our adaptive mirror were measured with an interferometer and the interferograms were then analysed with a commercially available software to attain the Zernike coefficients. The reconstructed interferograms of the response functions are shown in Fig. 6.

The defocus actuator (electrode no. 1), which covers the complete mirror aperture deforms the surface considerably stronger than all the other actuators. By applying the maximum positive voltage of 150 V to electrode no. 1 the surface forms a convex mirror with a radius of curvature of approximately 210 m. This corresponds to a stroke of 1 μm in the centre of the mirror. The maximum deflection for a voltage of −150 V was measured to be about 2.2 μm which results in a radius of curvature of 96 m. Due to the smaller area of the actuators no. 2 to no. 6 compared to electrode no. 1, the deflection caused by these electrodes is significantly lower. The influence of electrode no. 6 is even smaller because the mirror substrate is fixed at the outer border to the housing. Without any voltage applied the surface forms a concave mirror with a radius of curvature of approximately 420 m. This is equivalent to a peak to valley value of about 0.5 μm. By applying a voltage of +63 V to electrode no. 1 this deformation can easily be corrected, as shown in Fig. 7 on the right side.

| $j$ | $n$ | Zernike polynomial | Name |
|---|---|---|---|
| 0 | 0 | 1 | Constant |
| 3 | 2 | $2r^2-1$ | Defocus |
| 8 | 4 | $6r^4-6r^2+1$ | Primary spherical |
| 15 | 6 | $20r^6-30r^4+12r^2-1$ | Secondary spherical |
| 24 | 8 | $70r^8-140r^6+90r^4-20r^2+1$ | Tertiary spherical |

**TABLE 1** Angle-independent Zernike polynomials. Please note that the normalization is omitted

The optimum profile calculated in Sect. 2 can now be approximated with a linear combination of the measured response functions. The total surface deformation $z(r)$ can be written as an expansion of the response functions $F_i(r)$:

$$z(r) = z_0 + \sum_{i=1}^{N} U_i F_i(r) \tag{15}$$

with $U_i$ being the voltages which have to be applied to the electrodes and with the initial surface deformation $z_0$ (see Fig. 7, left side). $N$ is the number of actuators. The voltages $U_i$ which form the desired surface were found by using a least square fit to the phase front of the custom mode. We note that the voltage distribution which forms a given surface deformation is not unique. A very good approximation of the mirror surface to the phase front of the super-Gaussian mode was found with $U_0 = 61$ V, $U_1 = 21$ V, $U_2 = 150$ V, $U_3 = -140$ V, $U_4 = -150$ V and $U_5 = -150$ V (see Fig. 4, dotted line). Only at the edge of the mirror where the intensity of the beam decreases the profile deviates slightly from the optimum surface deformation. The calculation of the eigenmode – as described in Sect. 2 – confirmed that such a mirror profile will generate a mode which is close to the desired beam (see Fig. 1).

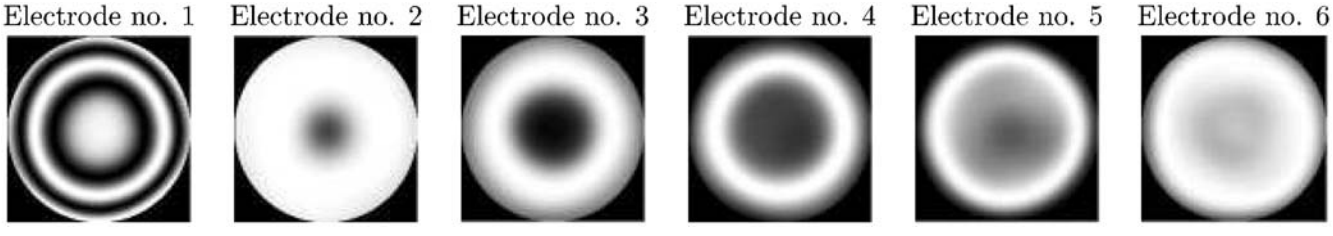


**FIGURE 6** The response functions of the adaptive mirror are shown as reconstructed interferograms. A voltage of 100 V was applied to each electrode. *The first interferogram on the left* depicts the response function of the defocus electrode (no. 1) which spans over the whole mirror surface. The *next five interferograms* show the surface deformation of the individual ring actuators (no. 2 to no. 6). The initial surface deformation is subtracted from all the acquired interferograms

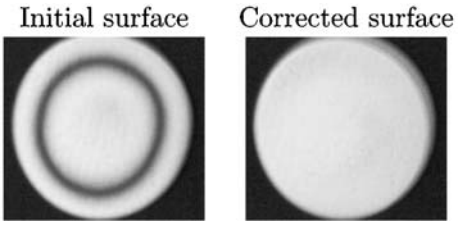


**FIGURE 7** Measured interferograms of the initial surface (*left*) and the corrected surface (*right*) of the adaptive mirror. All electrodes were grounded to acquire the interferogram of the uncontrolled surface. A positive voltage of 63 V applied to the defocus electrode (no. 1) corrects the initial curvature of the mirror surface

In the next section the voltage distribution which is needed to generate the requested beam is applied to the controllable mirror and we will discuss the resulting mode.

## 5 Experiments and results

All experiments were performed with a prototype transversally diode-pumped Nd:YAG laser. The diameter of the rod was 4 mm and the length was 30 mm. A threefold pump geometry yields an almost homogenous pump distribution over a radius of about 1 mm and decreases linearly for larger radii. Since only this central part of the gain was used to avoid aberrating modulations, the overall efficiency of the investigated laser was not very high but can easily be improved with further optimisation of the pumping distributions. It is important that the phase front is not deteriorated by thermal distortions because we did not consider thermally induced aberrations in the calculations. Therefore we carried out the experiments with quasi-CW pumping to minimise the thermal load of the laser rod. The quasi-CW laser diode driver (SDL 928-50) was set to a pulse duration of 500 µs and to a repetition rate of 30 Hz. The low duty cycle of 1.5% guarantees that there is enough time between the pulses to remove the heat.

The laser resonator consisted of the adaptive mirror on one end, followed by a Galilei telescope, the gain medium and a plane output coupler ($R = 90\%$) on the other end (see Fig. 3). The intracavity telescope increased the beam size on the adaptive mirror to exploit the entire deformable surface. The focal lengths of the telescope lenses were −60 mm and 600 mm resulting in a magnification factor of 10. The lenses were AR-coated at the laser wavelength.

To generate a super-Gaussian mode some of the calculated voltages (see Sect. 4) had to be modified most probably due to a non-perfect alignment of the telescope. By applying 22, −15, 150, 98, −150 and −150 V to electrodes no. 1 to 6, respectively, the adaptive mirror formed a super-Gaussian beam. The mirror surface which corresponds to this voltages distribution is illustrated in Fig. 4 as a dashed line. The measured super-Gaussian near-field intensity is shown in Fig. 8 as a solid line for a pump pulse energy of 123 mJ. The inset depicts the two-dimensional intensity distribution of the mode. The beam features a high rotation symmetry without any hot spots. Compared to the perfect super-Gaussian mode of the sixth order the observed super-Gaussian beam features a slightly lower super-Gaussian order most probably due to a non-perfect alignment of the intracavity telescope, due to the mechanical limitations of the mirror surface deformation and due to diffraction at the edge of the adaptive mirror. Considering that the modification of the phasefront is in the subwavelength range of the laser beam the calculated eigenmode and the measured mode correspond astoundingly well.

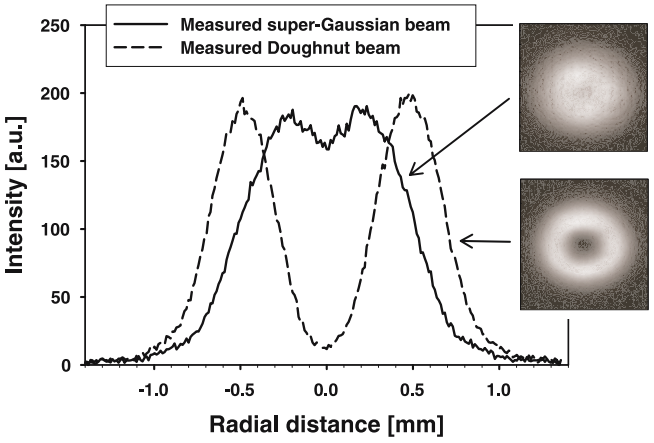


**FIGURE 8** Measured super-Gaussian and doughnut nearfield intensity distributions drawn as a *solid* and a *dashed line*, respectively. The *inset plots* show the two dimensional intensity distributions of the modes

We measured output energies per pulse of 0.6, 1.8, 3.4, 4.9, 6.4 and 8.0 mJ for pump pulse energies of 36, 53, 71, 88, 105 and 123 mJ, respectively. With the above-mentioned repetition rate of 30 Hz we get average powers of 19, 55, 100, 145, 192 and 239 mW. A slope efficiency of 8.6% and a second moment radius of 0.73 mm was determined. Note that this is a single mode and not an incoherent superposition of several modes. This was confirmed by measuring the beam propagation factor $M^2$ of the laser mode. The measured $M^2$ value of 1.6 agrees well with the theoretical value of 1.3 (for $n = 6$) [2–4]. No aperture was needed to prevent the oscillation of higher-order modes.

By changing the voltages to 40, −150, 150, 126, −34 and −150 V for the electrodes no. 1 to 6, respectively, the adaptive mirror formed a very stable doughnut beam. The mode was remarkably insensitive to variations of the control voltages. A typical mirror shape for the generation of a doughnut mode is shown in Fig. 9 as a solid line.

The measured nearfield intensity distribution of the doughnut mode is shown in Fig. 8 as a dashed line for a pump pulse energy of 123 mJ. The inset depicts the two-dimensional intensity distribution of the mode which features a high rotation symmetry and nearly zero intensity in the centre of the beam.

The following output energies per pulse were achieved: 1.0, 2.7, 4.7, 6.7, 8.8 and 11.0 mJ for pump pulse energies of 36, 53, 71, 88, 105 and 123 mJ, respectively. This results in average powers of 29, 81, 140, 200, 264 and 330 mW. Compared to the super-Gaussian mode a higher slope efficiency of 11.7% was attained due to the larger second moment radius of 0.90 mm. A $M^2$ value of 2.6 was determined. The deformable mirror inhibits the $TEM_{00}$ mode because of the convex shaped centre of the mirror surface.

A voltage of −93 V applied to electrode no. 1 and all other voltages set to zero shaped a fundamental Hermite–Gaussian mode ($TEM_{00}$). The adaptive mirror formed a concave mirror whose shape is drawn in Fig. 9 as a short-dashed line. No

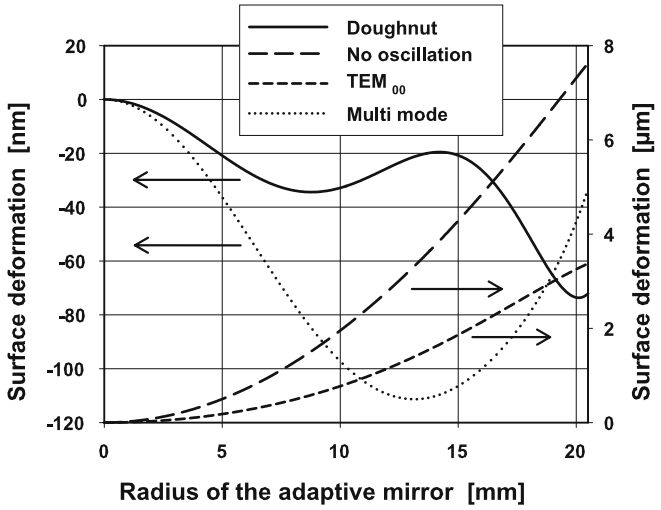


**FIGURE 9** The surface deformations which generated the $TEM_{00}$ mode, the multi mode beam and the doughnut mode were measured with an interferometer and reconstructed. The mirror shape which inhibited the oscillation of the laser is drawn as a *long-dashed line*

aperture was needed to prevent the oscillation of the higher-order modes. The low $M^2$ value of 1.4 confirmed that only one single transversal mode is present in the cavity. At a pump pulse energy of 123 mJ an output energy per pulse of 5.8 mJ was measured. We determined a slope efficiency of 6.1% and a second moment radius of 0.43 mm for the fundamental Gaussian mode.

The maximum output energy of 14.4 mJ was achieved with the following voltage distribution: 52, −150, −96, 150, 70 and 30 V applied to electrodes no. 1 to 6, respectively. This voltage distribution formed a mirror surface as shown in Fig. 9 as a dotted line. According to the comparatively high $M^2$ value of 5.1 several low order transversal modes had enough gain to oscillate in the resonator. We determined a slope efficiency of 15.8 % and a second moment radius of 1.09 mm.

To prevent laser oscillation completely we applied, for example, −150 V to electrode no. 1, −90 V to electrode no. 2 and 0 V to the other electrodes. This set of voltages shaped a concave mirror with a comparatively small radius of curvature of 27 m (see Fig. 9, long-dashed line). The g-parameter product of $-1.92$ falls below the value of 0, and therefore the resonator gets unstable. Of course the instability can be reached also with other sets of voltages.

We observed a temporally unstable oscillation of the $TEM_{00}$ mode in the region between the above surface profile, which suppresses laser operation and the surface profile for the stable generation of the $TEM_{00}$ mode.

## 6 Conclusion and outlook

Deformable mirrors are very versatile beam shaping elements which allow to change the intensity distribution of the mode in real time. Super-Gaussian beams as well as doughnut modes with a wavelength of 1064 nm were generated in a Nd:YAG laser by means of a semipassive bimorph adaptive mirror. A few actuators were enough to shape the beam towards two exemplary custom modes. The controllable mirror can also switch between the Hermite–Gaussian fundamental mode and the multi-mode regime or inhibit the laser oscillation in the resonator.

Beam shaping mirrors for the generation of custom modes may be combined with the self-adaptive compensation for thermal lenses [29, 30] in future experiments. In a CW-pumped laser systems the compensating element corrects the main contribution (i.e., the second order aberration) of the phase front deformation. In combination with the adaptive mirror the compensating element corrects the second order aberration and the adaptive mirror could reduce the higher-order aberrations and shape the beam.

The development of novel thermo-optical and thermo-mechanical adaptive devices is in progress [31–33]. We expect a high lateral resolution and large phase shifts in the range of 20 diopters.

**ACKNOWLEDGEMENTS** The authors thank H.P. Weber for fruitful discussion, Yulia V. Sheldakova for the measurements with the interferometer and Eva Krähenbühl for technical assistance.

## REFERENCES

1 N. Hudgson, H. Weber, *Optical Resonators* (Springer, London 1997)
2 A.E. Siegman, *New developments in laser resonators*, in: *Laser resonators*, vol. 1224 (Proc. Soc. Photo-Opt. Instrum. Eng. 1990), pp. 2–14
3 P. Bélanger, Beam propagation and the ABCD ray matrices, Opt. Lett. **16**, 196 (1991)
4 C. Paré, P. Bélanger, Beam propagation in a linear or nonlinear lens-like medium using the ABCD ray matrices: the method of moments, Opt. Quantum Electron. **24**, 1051 (1992)
5 W. Bloehs, F. Dausinger, *Shaping systems for hardening with high-power Nd:YAG-lasers*, in: *Proceedings of the 6th European Conference on Laser Treatment of Materials* (ECLAT '96, Stuttgart 1996)
6 R. Craxton, High efficiency frequency tripling schemes for high-power Nd:glass lasers, IEEE J. Quantum Electron. **QE-17**, 1771 (1981)
7 A. Siegman, *Lasers* (University Science Books, Mill Valley, CA 1986)
8 P. Bélanger, C. Paré, Optical resonators using graded-phase mirrors, Opt. Lett. **16**, 1057 (1991)
9 C. Paré, P. Bélanger, Custom laser resonators using graded-phase mirrors: Circular geometry, IEEE J. Quantum Electron. **QE-30**, 1141 (1994)
10 A. Napartovich, N. Elkin, V. Troschieva, D. Vysotsky, J. Leger, Simplified intracavity phase plates for increasing laser-mode discrimination, Appl. Opt. **38**, 3025 (1999)
11 J. Leger, D. Chen, Z. Wang, Diffractive optical element for mode shaping of a Nd:YAG laser, Opt. Lett. **19**, 108 (1994)
12 P. Bélanger, R. Lachance, C. Paré, Super-gaussian output from a $CO_2$ laser by using a graded-phase mirror resonator, Opt. Lett. **17**, 739 (1992)
13 R. van Neste, C. Paré, R. Lachance, P. Bélanger, Graded-phase mirror resonator with a super-gaussian output in a cw-$CO_2$ laser, IEEE J. Quantum Electron. **QE-30**, 2663 (1994)
14 M. Gerber, T. Graf, Generation of super-gaussian modes in Nd:YAG lasers with a graded-phase mirror, IEEE J. Quantum Electron. **QE-40**, 1 (2004)
15 B. Wattellier, J. Fuchs, J.-P. Zou, J.-C. Chanteloup, H. Bandulet, P. Michel, C. Labaune, S. Depierreux, A. Kudryashov, A. Aleksandrov, Generation of a single hot spot by use of a deformable mirror and study of its propagation in an underdense plasma, J. Opt. Soc. Am. B **20**, 1632 (2003)
16 A. Kudryashov, T. Cherezova, L. Kaptsov, *Adaptive optical system for control of the cw technological* YAG:$Nd^{3+}$ *laser beam parameters*, in: *High-power gas and solid state lasers*, vol. 2206 (Proc. SPIE, Europto Series 1994), pp. 574–576
17 T. Cherezova, L. Kaptsov, A. Kudryashov, Cw industrial rod YAG:$Nd^{3+}$ laser with an intracavity active bimorph mirror, Appl. Opt. **35**, 2554 (1996)
18 W. Lubeigt, G. Valentine, J. Girkin, E. Bente, D. Burns, Active transverse mode control and optimisation of an all-solid-state laser using an intracavity adaptive-optic mirror, Opt. Express **10**, 550 (2002)
19 U. Wittrock, I. Buske, H. Heuck, *Adaptive aberration control in laser amplifiers and laser resonators*, in: *Laser Resonators and Beam Control VI*, vol. 4969 (Proc. SPIE 2003), pp. 122–136

20 F. Gonté, A. Courteville, R. Dändliker, Optimization of single-mode fiber coupling efficiency with an adaptive membrane mirror, Opt. Eng. **41**, 1073 (2002)
21 J. Liang, D. Williams, D. Miller, Supernormal vision and high-resolution retinal imaging through adaptive optics, J. Opt. Soc. Am. A **14**, 2884 (1997)
22 T. Cherezova, S. Chesnokov, L. Kaptsov, V. Samarkin, A. Kudryashov, Active laser resonator performance: formation of a specified intensity output, Appl. Opt. **40**, 6026 (2001)
23 J. Leger, D. Chen, G. Mowry, Design and performance of diffractive optics for custom laser resonators, Appl. Opt. **34**, 2498 (1995)
24 S. Makki, J. Leger, Mode shaping of a graded-reflectivity mirror unstable resonator with an intracavity phase element, IEEE J. Quantum Electron. **QE-37**, 80 (2001)
25 A. Kudryashov, V. Shmalhausen, Semipassive bimorph flexible mirrors for atmospheric adaptive optics applications, Opt. Eng. **35**, 3064 (1996)
26 M. Born, E. Wolf, *Principles of optics* (Cambridge University Press 1999)
27 J. Wang, D. Silva, Wave-front interpretation with zernike polynomials, Appl. Opt. **19**, 1510 (1980)
28 R.J. Noll, Zernike polynomials and atmospheric turbulence, J. Opt. Soc. Am. **66**, 207 (1976)
29 R. Weber, T. Graf, H. Weber, Self-adjusting compensating thermal lens to balance the thermally induced lens in solid-state lasers, IEEE J. Quantum Electron. **QE-36**, 757 (2000)
30 E. Wyss, M. Roth, T. Graf, H. Weber, Thermooptical compensation methods for high-power lasers, IEEE J. Quantum Electron. **QE-38**, 1620 (2002)
31 D. Michel, T. Graf, H. Glur, W. Luethy, H. Weber, Thermo-optically driven adaptive mirror for laser applications, Appl. Phys. B **77**, 721 (2004)
32 F. Reinert, T. Graf, W. Luethy, H. Weber, Optically controlled adaptive mirror, Laser Phys. Lett. **1**, 551 (2004)
33 E. Wyss, T. Graf, *Verfahren, Anordnung und Beeinflussungseinheit fuer die Anordnung zur Veraenderung einer Wellenfront eines optischen Strahls*, EU Patent 03 405 128.4, 2003